physica status solidi rrl
www.pss-rapid.com

Check for updates

# High-Performance and Stable Dopant-Free Silicon Solar Cells with Magnesium Acetylacetonate Electron-Selective Contacts

*Zhirong Yao, Lun Cai, Lanxiang Meng, Kaifu Qiu, Wenjie Lin, Jingsheng Jin, Weiyuan Duan, Kaining Ding, Shenghao Li,* Bin Ai, Zongcun Liang, and Hui Shen**

**One of the challenges in fabricating high-performance n-type crystalline silicon (n-type c-Si) solar cells is the high-quality n-type c-Si/metal contact. Schottky barriers are commonly found on the n-type c-Si/metal contact, which suppresses electron transportation. Herein, novel stacks of magnesium acetylacetonate ($Mg(Acac)_2$)/magnesium (Mg)/silver (Ag) to form electron-selective contacts for n-type c-Si solar cells are presented, which enables a dopant-free process. An ohmic contact on n-type c-Si is formed using the $Mg(Acac)_2$/Mg/Ag stacks. The transmission spectrum and ultraviolet photoelectron spectroscopy measurements show negligible conduction-band offset and large valence-band offset between $Mg(Acac)_2$ and n-type c-Si, which indicates the electron-transporting and hole-blocking properties of $Mg(Acac)_2$/n-type c-Si heterocontacts. Moreover, the contact resistivities ($\rho_c$) between the $Mg(Acac)_2$/Mg/Ag electron-selective heterocontacts and n-type c-Si substrates are lower than 10 $m\Omega\,cm^2$, which demonstrates the good electrode properties of the $Mg(Acac)_2$/Mg/Ag stacks. The $Mg(Acac)_2$/Mg/Ag electron-selective stacks are applied on n-type c-Si solar cells with partial rear contact, and >20% efficiency is achieved, which is higher than that in a reference cell with only Ag contact. The stability of the n-type c-Si solar cell performance equipped with $Mg(Acac)_2$/Mg/Ag contacts is verified under ambient conditions. This novel low-temperature contact technique offers a reliable alternative for high-performance n-type c-Si solar cells.**

By improving silicon (Si) wafer quality and reducing production cost, Si solar cells have become a dominating product in the global photovoltaic market with a market share of over 90%. Currently, most of the Si solar cells in the market are based on p-type Czochralski-grown crystalline silicon (p-type Cz c-Si) wafers with a front phosphorus-diffused emitter and a local or full-area aluminum (Al)-alloyed rear contact.[1] In these solar cells, heavily Al-doped Al–Si alloy layers are formed during a high-temperature firing, which gives rise to metal–Si contacts with low contact resistances. However, in p-type Cz c-Si wafers, the carrier lifetimes are susceptible to metastable boron- and oxygen-related defect center.[2,3] Accordingly, there has been considerable interest on n-type Cz c-Si wafers, because they have a high carrier lifetime and no light-induced degradation related to the boron- and oxygen-related defects.[4–6] Using n-type substrates, a world-record 26.7% energy conversion efficiency ($\eta$) of Si heterojunction solar cells with interdigitated back contacts was reported by Yoshikawa et al. in 2017.[5] The direct contacts between n-type c-Si and Al or silver (Ag) are non-ohmic, and forming excellent metal–Si contacts on lightly doped n-type c-Si still remains a challenge.[7] In the industry, phosphorous diffusion and plasma immersion ion implantation have been introduced to form heavily doped $n^{++}$ areas to ensure a low contact resistivity between n-type c-Si and metals.[8,9] Nevertheless, phosphorous diffusion and plasma immersion ion implantation include ≈900 °C

Z. Yao, Dr. L. Cai, L. Meng, Dr. K. Qiu, W. Lin, Dr. S. Li, Prof. B. Ai, Prof. Z. Liang, Prof. H. Shen
Institute for Solar Energy Systems
Guangdong Provincial Key Laboratory of Photovoltaic Technology
School of Physics
Sun Yat-sen University
510006 Guangzhou, P. R. China
E-mail: shenhui1956@163.com

The ORCID identification number(s) for the author(s) of this article can be found under https://doi.org/10.1002/pssr.202000103.



**DOI: 10.1002/pssr.202000103**

Z. Yao, Dr. K. Qiu, Dr. W. Duan, Dr. K. Ding, Dr. S. Li
IEK-5 Photovoltaik
Forschungszentrum Jülich
Leo-Brandt-Straße, 52425 Jülich, Germany
E-mail: s.li@fz-juelich.de

Dr. J. Jin
R&D Centre
Jinko Solar Holding Co. Ltd.
Yuanhua Town, 314416 Haining, P. R. China

Prof. H. Shen
Jiangsu Collaborative Innovation Center of Photovoltaic Science and Engineering
Changzhou University
No. 1 Gehu Road, 213164 Changzhou, P. R. China

high-temperature treatments, which give rise to a high energy consumption. Moreover, heavy doping in Si results in $\eta$ loss due to extra Auger recombination and free carrier absorption.[10,11]

Another solution for n-type c-Si contacts is the application of electron-selective materials. Low-work-function materials (e.g., lithium fluoride (LiF)[12,13] and magnesium (Mg)[14]) or materials with small conduction-band offsets with Si ($TaN_x$) are applied as electron-selective materials in n-type c-Si contacts.[15] In addition, oxides play a vital role in selective contacts, such as $TiO_x$ and ZnO.[16,17] N-type c-Si solar cells using $TiO_x$/$LiF_x$/Al electron-selective heterocontacts exhibit a low contact resistivity of $\approx$5 m$\Omega$ cm$^2$ and achieved 23% energy conversion efficiency in a recent study.[18] However, low-work-function materials, such as LiF, suffer from instability in ambient environments. Thus, a stable electron-selective contact for n-type c-Si with a simple fabrication process is still of great interest. Bullock et al. reported dopant-free asymmetric heterocontact Si solar cells with efficiencies above 20% using a $TiO_x$ insert layer between c-Si and LiF/Ag. This triple layer ensures a thermal stability of c-Si solar cells after undergoing 300 °C post-annealing treatment.[19]

Metal acetylacetonates have been used as stable electron-selective heterocontacts for perovskite solar cells.[20] In this work, we present a novel contact technique for electron-selective contacts on n-type c-Si solar cells using a magnesium acetylacetonate ($Mg(Acac)_2$) insert layer between n-type c-Si and Ag that features ambient stability. The $Mg(Acac)_2$ organic material serving as an insert layer between n-type c-Si and Mg is introduced here to achieve stable and high-quality electron-selective contacts for the first time. Moreover, the electronic band structure and application of n-type c-Si solar cells in the thermal-evaporated $Mg(Acac)_2$/Mg/Ag stacks are discussed. The stability of proof-of-concept contact structure and performance discrepancy with different contacts is revealed. This study aims at closing the gap between high-performance n-type c-Si solar cell devices and stable dopant-free contacts with a simplified process and presents the first results of $Mg(Acac)_2$ on n-type c-Si solar cells.

The atomic structure of $Mg(Acac)_2$ is shown in **Figure 1**a. $Mg(Acac)_2$ films (12 nm) were evaporated on n-type c-Si (100) substrates (1–3 $\Omega$ cm) for the X-ray photoelectron spectroscopy (XPS) characterization to obtain the bonding information of Mg(Acac). The chemical states of Mg, C, and O in $Mg(Acac)_2$ studied by XPS are shown in Figure 1b–d. The Mg1s spectrum exhibits a typical peak at 1303.1 eV.[21] The peak analysis of the C1s spectrum shows the presence of four bonding types of the carbon atoms. Two predominant peaks at 285.1 and 284.2 eV are attributed to $sp^3$ C—C and $sp^2$ C=C bonds, and the peaks at $\approx$289.0 and 286.7 eV are attributed to the C=O and C—O bonds.[22] In the O1s XPS spectrum, the peaks of the O—Mg (532.4 eV), C=O (531.3 eV), and C—O (530.1 eV) bonds are observed.[23] All of the bonds in $Mg(Acac)_2$ are found in the XPS spectra. The atomic ratio of Mg:C:O is $\approx$5:16:12, which is not close to that of the raw $Mg(Acac)_2$ powder, which is 1:5:2. Some of the missing C may be oxidized by rare $O_2$ in the chamber during the $Mg(Acac)_2$ thermal evaporation process.

To study the mechanisms underlying the electron-selective transport of the $Mg(Acac)_2$/n-type c-Si heterocontact, the band alignment at the $Mg(Acac)_2$/n-type c-Si interface was investigated. A fit was applied in the transmittance spectrum of $Mg(Acac)_2$, giving an optical bandgap value ($E_g$) of 3.9 eV, as shown in

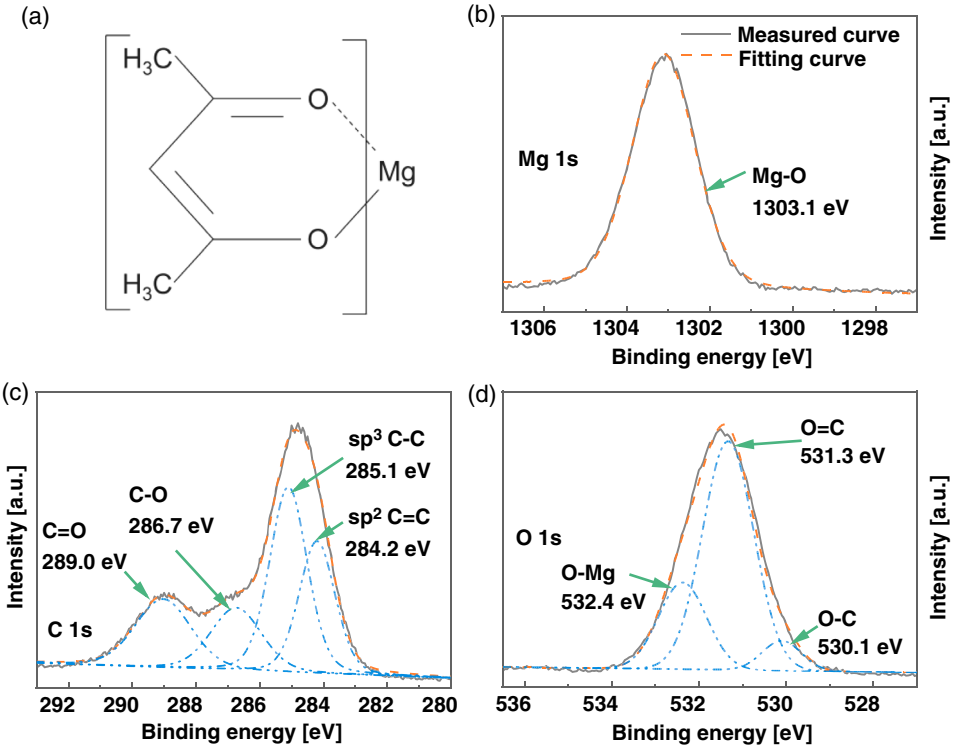


**Figure 1.** a) Molecular structure of $Mg(Acac)_2$. XPS spectra of the $Mg(Acac)_2$ sample: b) Mg1s, c) C1s, and d) O1s.

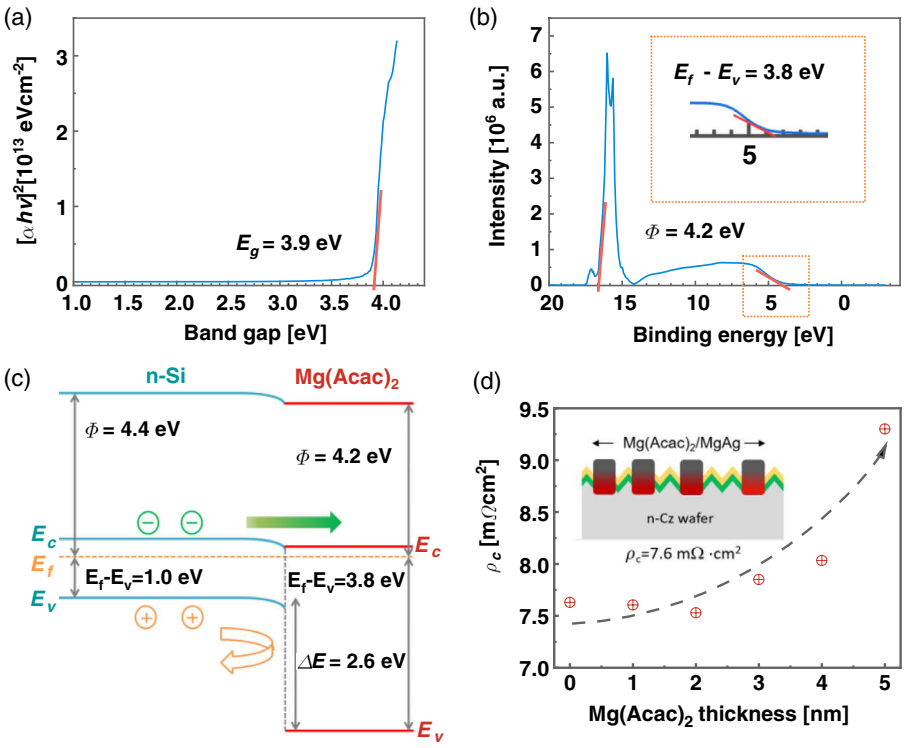


**Figure 2.** a) Determination of the optical bandgap from the transmittance spectrum for the $Mg(Acac)_2$. b) UPS spectrum of the $Mg(Acac)_2$ film using He I excitation; a zoom for the $E_f$–$E_v$ value linear fit is included in the inset. c) Band alignment at the n-type c-Si/$Mg(Acac)_2$ interface. d) $\rho_c$ as a function of the $Mg(Acac)_2$ thickness; TLM pattern structure is included in the inset.

**Figure 2**a. Figure 2b shows the ultraviolet photoelectron spectroscopy (UPS) spectrum of the $Mg(Acac)_2$ thin film using a He I excitation (21.22 eV). The work function ($\Phi$) of $4.2 \pm 0.05$ eV was calculated by considering the onset ($16.9 \pm 0.05$ eV) in the UPS spectrum at high binding energy.[15] The gap between the Fermi level and valence band maximum ($E_f - E_v$) in $Mg(Acac)_2$, obtained from the linear fit in the UPS spectrum with the inset, is $3.8 \pm 0.05$ eV. The work function and ($E_f - E_v$) values of the Si substrate are 4.4 and 1.0 eV, respectively, obtained from the UPS spectrum.[15]

The band alignment diagram at the $Mg(Acac)_2$/n-type c-Si interface shows carrier selectivity, as shown in Figure 2c. Two desirable properties of this $Mg(Acac)_2$ insert layer are demonstrated: 1) a negligible conduction-band offset between the n-type c-Si and $Mg(Acac)_2$ layer, which enables the free transport of electrons and 2) a large valence-band offset ($\Delta E_v = 2.6$ eV), which effectively blocks the hole transportation. The efficient electron transportation of the $Mg(Acac)_2$/Mg/Ag structure can be addressed by its contact resistivity via the transfer length method (TLM). To evaluate the performance of the n-type c-Si/$Mg(Acac)_2$ heterocontact, the contact resistivity ($\rho_c$) with the different $Mg(Acac)_2$ thicknesses is measured by TLM, as shown in Figure 2d. The results show that $\rho_c$ increases as the thickness of the $Mg(Acac)_2$ layer increases. $\rho_c$ is below 10 mΩ cm$^2$ when the $Mg(Acac)_2$ layer is $\leq$5 nm, showing a promising contact for n-type c-Si. A high electron selectivity was demonstrated by the low contact resistivity.

N-type c-Si solar cells with a partial rear contact were fabricated to demonstrate the quality of the $Mg(Acac)_2$/Mg/Ag heterocontact on the device. Thermal $SiO_2$ growth and plasma-enhanced chemical vapor deposition (PECVD) of a $SiN_x$ passivation/dielectric spacer were patterned with 30 µm-diameter holes to the c-Si surface on the rear side. Through these holes, the $Mg(Acac)_2$/Mg/Ag stack contacted the n-type c-Si surface, directly forming the electron-selective contact shown in **Figure 3**a. The Ag/Mg/$Mg(Acac)_2$/n-type c-Si contact was observed via scanning transmission electron microscopy (STEM) acquired with a high-angle annular dark field (HAADF) in combination with energy-dispersive X-ray spectroscopy (EDX), as shown in Figure S1, Supporting Information. From the elemental mapping in Figure S1b, Supporting Information, a $Mg(Acac)_2$/Mg interlayer stack between Si and Ag is observed. $Mg(Acac)_2$ is too thin, making it difficult to distinguish with the Mg layer. The results highlight that the Mg and $Mg(Acac)_2$ layers separate the Si from the Ag layer. The oxygen signal in Figure S1c, Supporting Information, in the EDX mapping came from $Mg(Acac)_2$ as the material has a molecular structure, as shown in Figure 1a, which is consistent with the STEM observation.

Figure 3b shows the current density–voltage ($J$–$V$) plot of the champion cell with the 2 nm $Mg(Acac)_2$ layer. The solar cells achieved conversion efficiency $\eta$, open-circuit voltage ($V_{oc}$), and short-circuit current ($J_{sc}$) of 21.3%, 652.7 mV, and 41.42 mA cm$^{-2}$, respectively. A fill factor (FF) of 78.71% was achieved, showing the excellent collection of the hole and electron carriers. The low contact resistivity contributes to the high FF on the n-type c-Si solar cells. Stability is one of the crucial

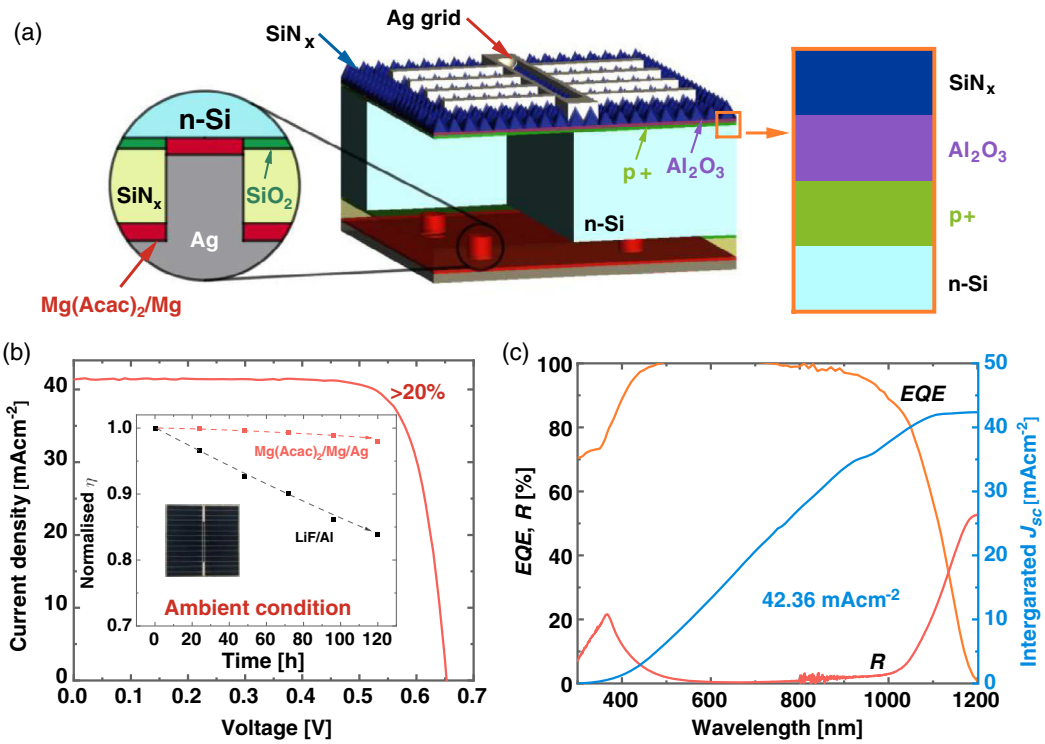


**Figure 3.** a) Schematic diagram of the n-type Si solar cell featuring partial rear $Mg(Acac)_2$/Mg/Ag carrier-selective heterocontacts. Schematics of $Mg(Acac)_2$/Mg/Ag partial rear contact structure and solar cell front side are included in the left and right insets, respectively. b) Champion solar cell performance with partial rear $Mg(Acac)_2$ electron-selective heterocontacts. Comparisons of the device stabilities for the n-type c-Si solar cells with the $Mg(Acac)_2$/Mg/Ag heterocontact and LiF/Al contact are included in the inset. c) EQE and reflectance for the champion solar cell with the $Mg(Acac)_2$ insert layer.

properties for solar cells. The solar cells with $Mg(Acac)_2$/Mg/Ag heterocontacts were investigated at 25 °C in an ambient environment. The *J*–*V* curves were periodically measured to extract device parameters. In the inset of Figure 3b, no significant change in the $Mg(Acac)_2$/Mg/Ag heterocontact solar cell performance, which maintained more than 97.8% of $\eta$, can be observed over the specified period. As a comparison, the performance of the reference cell using LiF/Al electrodes rapidly degraded to 83.6% of $\eta$. This finding indicates that the $Mg(Acac)_2$/Mg/Ag contact shows good stability in an ambient environment. Figure 3c shows the external quantum efficiency (EQE), solar cell reflection spectrum (*R*), and integrated $J_{sc}$. In the EQE spectrum, a good carrier collection in the whole wavelength range of the n-type c-Si solar cells applying $Mg(Acac)_2$/Mg electron-selective contacts was demonstrated. Moreover, an integrated $J_{sc}$ of 42.36 mA cm$^{-2}$ was obtained from the EQE that was measured using a spot exclude grid, which shows a slight discrepancy with the values obtained via the *J*–*V* measurement considering ≈4% coverage of the front Ag contact. The actual $J_{sc}$ of the solar cells was close to 40.67 mA cm$^{-2}$; hence, an efficiency of champion cell is below 21.3% and above 20%. A possible reason for this discrepancy is attributed to the calibration issue of the current–voltage tool. The measured *J*–*V* results are still suitable for the comparison of different cell performances with varying rear contact stacks as they are performed under the same test conditions.

**Table 1** shows the champion solar cell performance with $V_{oc}$, FF, $J_{sc}$, and $\eta$ using different rear contact stacks. Wan et al.

**Table 1.** Champion solar cell performance with different rear contacts.

| Rear contacts | $V_{oc}$ [mV] | FF [%] | $J_{sc}$ [mA cm$^{-2}$] | $\eta$ [%] |
|---|---|---|---|---|
| Ag | 652.8 | 77.16 | 40.83 | 20.6 |
| Mg/Ag | 649.8 | 77.76 | 41.26 | 20.9 |
| $Mg(Acac)_2$/Mg/Ag | 652.7 | 78.71 | 41.42 | 21.3 |

believed that a poor electron transport to electrode is suffered in the n-type c-Si/Ag contact due to the rectifying contact at the rear side, although the cell without the Mg layer has a similar carrier generation and recombination.[14] Moreover, a low $J_{sc}$ was obtained in the direct Ag contact in this study. Mg was inserted between n-type c-Si and Ag to achieve an ohmic contact, resulting in a high $J_{sc}$ of 41.26 mA cm$^{-2}$. Mg has one of the lowest work functions in metals, making it very suitable in forming an electron-conductive contact for Si solar cells.[14,21] Wu et al. suggested that recombination can be suppressed by introducing low-work-function metals to obtain a high $J_{sc}$.[24] High-quality electron selectivity was achieved by reducing recombination from the direct metal–semiconductor contact and high-performance n-type c-Si solar cells with a $Mg(Acac)_2$ insert layer. $Mg(Acac)_2$/Mg/Ag stacks improved solar cells' $\eta$ from 20.6% to 21.3% compared with the direct Ag contact, which resulted in a higher $J_{sc}$. A higher EQE in the 400–900 nm wavelength region with the $Mg(Acac)_2$/Mg/Ag stack was compared with

the Ag contact shown in Figure S2c, Supporting Information, which demonstrates that a better carrier collection was performed by the $Mg(Acac)_2$/Mg/Ag electron-selective contact even though the exact mechanism is still unclear. Chee revealed that the electron affinity, surface band bending, and charge transfer properties are changed because of the strong surface work function dependence on the Si surface.[25] Therefore, carriers are more easily extracted from the Si substrate by applying low-work-function $Mg(Acac)_2$/Mg/Ag contacts that gave a low contact resistivity, high $J_{sc}$, and high EQE.

In conclusion, we present stable dopant-free $Mg(Acac)_2$/Mg/Ag stacks as electron-selective heterocontacts for n-type c-Si. Fabricated in room temperature, the n-type c-Si/$Mg(Acac)_2$/Mg/Ag contacts showed a low contact resistivity below 10 mΩ cm$^2$. The band alignment analysis results extracted from the transmittance spectrum and UPS measurements show an electron-selective property between n-type c-Si and $Mg(Acac)_2$. Moreover, ambient stability was demonstrated in the solar cells with the $Mg(Acac)_2$/Mg/Ag electron-selective heterocontacts. These results prove that the $Mg(Acac)_2$/Mg/Ag stacks can be alternatives for an n-type c-Si contact in high-performance solar cells because of their good contact, simple process, and good stability.

## Experimental Section

XPS (Escalab 250Xi, Thermo Fisher Scientific, Waltham, MA, USA) was performed to characterize the components of $Mg(Acac)_2$. UPS measurements (Escalab 250Xi using the monochromated He I radiation [21.2 eV]) were used to determine the valence band and work function of $Mg(Acac)_2$. For the XPS and UPS characterization, 12 nm $Mg(Acac)_2$ films were evaporated on n-type c-Si (100) substrates (1–3 Ω cm). Ar etch (2 min) for the sample surface was conducted to clean the sample surface before the UPS and XPS measurements. $Mg(Acac)_2$ (30 nm) was deposited on 1.1 mm-thick Corning Eagle glass for the transmission measurement. The optical properties were obtained using a UV–vis–NIR spectrophotometer (U4100, HITACHI), and the wavelength step was 1 nm from 300 to 1200 nm. To fabricate the electron-selective heterocontact, $Mg(Acac)_2$ films with different thicknesses were deposited on the n-type Cz c-Si surface (1.0 Ω cm) at room temperature via thermal evaporation. A growth rate of ≈0.1 Å s$^{-1}$ was used for the deposition. Following this, Mg (≈10 nm)/Ag (≈300 nm) metal stacks were evaporated in the same system. The purity of $Mg(Acac)_2$ used in this study is 99.9%. Then, 99.99% Mg and Ag particles were used to deposit the metal electrode. Thermal evaporation depositions were conducted with a base chamber pressure of ≈$8 \times 10^{-4}$ Pa. The distance from the source to the substrate is 38 cm. Deposition rates of 0.50 and 0.50 nm s$^{-1}$ were used for Mg and Ag, respectively. The film thickness of $Mg(Acac)_2$ was determined by fitting polarized reflectance using the Tauc–Lorentz model in the spectroscopic ellipsometry measurement (SENTECH SE 800 PV ellipsometer).[26] The TLM for the contact resistivity measurement was carried out with a Keithley 2000 source meter.

N-type Cz c-Si wafers with a resistivity of 1.0 Ω cm and a thickness of 180 μm were used for solar cell fabrications. A homogeneous $p^+$ emitter was formed by boron diffusion furnace after texturing and cleaning. The n-type c-Si solar cells were fabricated with double-boron diffusion on the front to create localized heavily doped $p^{++}$ regions under the front metal contacts. One-side wet bench was conducted for removing the rear $p^+$ region. An $Al_2O_3/SiN_x$ passivation and antireflection stack was deposited on the front side via atomic layer deposition and PECVD, respectively. The front contacts, which only took up ≈4% of the front surface, were conducted by screen-printing Ag paste and firing. A peak temperature of ≈770 °C was used for the firing process of the cells. Then, different stacks, such as direct Ag, Mg/Ag, and $Mg(Acac)_2$/Mg/Ag, were deposited by thermal evaporations with a partial rear contact via 30 μm-diameter holes opened by a picosecond laser. The fabrication process of the n-type solar cells with the $Mg(Acac)_2$/Mg/Ag selective contact is shown in Figure S3, Supporting Information. We measured the illuminated *J–V* behavior of the solar cells under standard 1 sun conditions (100 mW cm$^{-2}$, AM1.5 spectrum, 25 °C) using a solar simulator (Class AAA, Oriel Sol3A, Newport). Reflection measurements were performed using a double-beam spectrophotometer (Cary 5000, Agilent Technologies) in the range of 300–1200 nm. The EQE spectrum was measured in the direct current mode on a spectrum corresponding system (Enlitech QE-R). For the stability research, the solar cells were exposed in ambient air at room temperature without illumination and heating for 120 h, and the *J–V* measurement was performed after every 24 h. The cross section of the n-type c-Si/$Mg(Acac)_2$/Mg/Ag contact stack on the rear opening area was observed with a FEI (Field Electron and Ion Company) Titan Themis G2 200 STEM. STEM microscopy images were acquired with HAADF in combination with EDX.

## Supporting Information

Supporting Information is available from the Wiley Online Library or from the author.

## Acknowledgements

This work is supported by the National Natural Science Foundation of China (grant nos. 61774173 and 61774171); the Guangzhou Collaborative Innovation Major Project for production, teaching, and research (grant no. 201508010011); and the Jiangsu Collaborative Innovation Center of Photovoltaic Science and Engineering (grant no. SCZ1405500002). The authors gratefully acknowledge financial support from the China Scholarship Council.

## Conflict of Interest

The authors declare no conflict of interest.

## Keywords

dopant-free contacts, magnesium acetylacetonate, selective contacts, silicon solar cells, thin films

Received: March 2, 2020
Revised: April 12, 2020
Published online: April 27, 2020

[1] F. Fertig, R. Lantzsch, A. Mohr, M. Schaper, M. Bartzsch, D. Wissen, F. Kersten, A. Mette, S. Peters, A. Eidner, J. Cieslak, K. Duncker, M. Junghänel, E. Jarzembowski, M. Kauert, B. Faulwetter-Quandt, D. Meißner, B. Reiche, S. Geißler, S. Hörnlein, C. Klenke, L. Niebergall, A. Schönmann, A. Weihrauch, F. Stenzel, A. Hofmann, T. Rudolph, A. Schwabedissen, M. Gundermann, M. Fischer, et al., *Energy Procedia* **2017**, *124*, 338.
[2] F. E. Rougieux, B. Lim, J. Schmidt, M. Forster, D. MacDonald, A. Cuevas, *J. Appl. Phys.* **2011**, *110*, 063708.
[3] J. Schmidt, K. Bothe, *Phys. Rev. B* **2004**, *69*, 024107.
[4] G. Masmitjà, P. Ortega, J. Puigdollers, L. G. Gerling, I. Martín, C. Voz, R. Alcubilla, *J. Mater. Chem. A* **2018**, *6*, 3977.
[5] K. Yoshikawa, H. Kawasaki, W. Yoshida, T. Irie, K. Konishi, K. Nakano, T. Uto, D. Adachi, M. Kanematsu, H. Uzu, K. Yamamoto, *Nat. Energy* **2017**, *2*, 17032.
[6] D. Macdonald, L. J. Geerligs, *Appl. Phys. Lett.* **2004**, *85*, 4061.

[7] D. K. Schroder, *Semiconductor Material and Device Characterization*, Wiley, Hoboken, NJ, USA **2006**.
[8] W. Cai, S. Yuan, Y. Sheng, W. Duan, Z. Wang, Y. Chen, Y. Yang, P. P. Altermatt, P. J. Verlinden, Z. Feng, *Energy Procedia* **2016**, *92*, 399.
[9] A. Lanterne, J. Lerat, T. Michel, T. Desrues, M. Coig, F. Milesi, F. Mazen, Y. Veschetti, L. Roux, S. Dubois, presented at 44th IEEE Photovoltaic Spec. Conf., Washington, DC, June 2017.
[10] S. C. Baker-Finch, K. R. McIntosh, D. Yan, K. C. Fong, T. C. Kho, *J. Appl. Phys.* **2014**, *116*, 063106.
[11] A. Richter, S. W. Glunz, F. Werner, J. Schmidt, A. Cuevas, *Phys. Rev. B* **2012**, *86*, 165202.
[12] J. Bullock, Y. Wan, Z. Xu, S. Essig, M. Hettick, H. Wang, W. Ji, M. Boccard, A. Cuevas, C. Ballif, A. Javey, *ACS Energy Lett.* **2018**, *3*, 508.
[13] P. L. Janega, J. McCaffrey, D. Landheer, M. Buchanan, M. Denhoff, D. Mitchel, *Appl. Phys. Lett.* **1988**, *53*, 2056.
[14] Y. Wan, C. Samundsett, D. Yan, T. Allen, J. Peng, J. Cui, X. Zhang, J. Bullock, A. Cuevas, *Appl. Phys. Lett.* **2016**, *109*, 113901.
[15] X. Yang, E. Aydin, H. Xu, J. Kang, M. Hedhili, W. Liu, Y. Wan, J. Peng, C. Samundsett, A. Cuevas, S. De Wolf, *Adv. Energy Mater.* **2018**, *8*, 1800608.
[16] X. Yang, Q. Bi, H. Ali, K. Davis, W. V. Schoenfeld, K. Weber, *Adv. Mater.* **2016**, *28*, 5891.
[17] B. Murali, A. El Labban, J. Eid, E. Alarousu, D. Shi, Q. Zhang, X. Zhang, O. M. Bakr, O. F. Mohammed, *Small* **2015**, *11*, 5272.
[18] J. Bullock, Y. Wan, M. Hettick, X. Zhaoran, S. P. Phang, D. Yan, H. Wang, W. Ji, C. Samundsett, Z. Hameiri, D. Macdonald, A. Cuevas, A. Javey, *Adv. Energy Mater.* **2019**, *9*, 1803367.
[19] J. Bullock, Y. Wan, Z. Xu, S. Essig, M. Hettick, H. Wang, W. Ji, M. Boccard, A. Cuevas, C. Ballif, A. Javey, *ACS Energy Lett.* **2018**, *3*, 508.
[20] W. Chen, L. Xu, X. Feng, J. Jie, Z. He, *Adv. Mater.* **2017**, *29*, 1603923.
[21] Y. Wan, C. Samundsett, J. Bullock, M. Hettick, T. Allen, D. Yan, J. Peng, Y. Wu, J. Cui, A. Javey, A. Cuevas, *Adv. Energy Mater.* **2017**, *7*, 1601863.
[22] T. I. T. Okpalugo, P. Papakonstantinou, H. Murphy, J. McLaughlin, N. M. D. Brown, *Carbon (N.Y.)* **2005**, *43*, 153.
[23] B. Lai, F. Mei, Y. Gu, *Chem. – An Asian J.* **2018**, *13*, 2529.
[24] W. Wu, W. Lin, S. Zhong, B. Paviet-Salomon, M. Despeisse, Q. Jeangros, Z. Liang, M. Boccard, H. Shen, C. Ballif, *Phys. Status Solidi RRL – Rapid Res. Lett.* **2020**, *14*, 1900688.
[25] A. K. W. Chee, *IEEE Trans. Electron Devices* **2019**, *66*, 4883.
[26] G. E. Jellison, F. A. Modine, *Appl. Phys. Lett.* **1996**, *69*, 371.